IEEE Access
Multidisciplinary | Rapid Review | Open Access Journal

Received March 27, 2019, accepted April 22, 2019, date of publication April 30, 2019, date of current version May 20, 2019.

Digital Object Identifier 10.1109/ACCESS.2019.2913950

A Study on the Control of a Sensorless Pneumatic Joint Using Predictive Control Method

YANHENG ZHANG, (Member, IEEE), XIE CHEN, HUIZHI WANG, AND LUFENG ZHANG
Automation School, Beijing University of Posts and Telecommunications, Beijing 100876, China

Corresponding author: Yanheng Zhang (zyh620@bupt.edu.cn)

This work was supported by the Key Project of Chinese National Programs for Fundamental Research and Development (973 Program) under Grant 2013CB733000.

ABSTRACT In high voltage substations, motors and sensors of a manipulator are susceptible to strong electromagnetic interference (EMI) and cannot work normally. The pneumatic motor can be a good method to overcome this problem. We present a novel five degree-of-freedom (DOF) manipulator design which is driven by pneumatic motors with no angle sensors. This design is simple but effective, and it can make the manipulator possess the potential to withstand the ultra-high voltage. It is also insensitive to EMI in high voltage substation due to its sensorless structure. The dynamic model of the wrist joint is established, and the state space equation, in which the pressure loss is contained, is proposed. The experiments are performed under different air pressures to validate the accuracy of the angle prediction model. A closed-loop control method, in which the angle prediction model is used as a feedback signal, is developed for this sensorless wrist joint. Finally, the rotation experiments were applied to test the validity of this control method, and the results showed that this method can improve the controllability of this type of wrist joint.

INDEX TERMS Manipulators, pneumatic actuators, fluid dynamics, prediction methods.

I. INTRODUCTION

Live work on a distribution network is a high risk work. Many maintenance tasks are conducted by human workers. To improve the efficiency and prevent injury in the maintenance of power distribution lines, researchers have developed many types of robots [1]–[10].

Motors are the most common driving units used in live working robots. Researchers have studied this type of robots since 1995 [2]. Lima *et al.* [3] developed a power line maintenance system called ''POLIBOT''. This robot can operate on 207 kV live lines with multiturn servo motors. To detect faulty insulators in advance, a robot [4] with a better insulating property was developed. This motor driven robot uses a wheel-leg moving mechanism to enable it to move on the insulators. The robot can work on 375 kV power lines. Jiang *et al.* [5] introduced a type of motor driven live maintenance robot aimed at bolt tightening and insulator strings replacement. The robot system and its control method are verified by an actual 220 kV live operation experiments. Kiyoshi *et al.* [6] proposed an experimental robot system for line maintenance. The experimental system consists of a robot arm (Mitsubishi Electric model RV-1A), a vehicle and a camera. The system can achieve a ''bolt insertion'' task by visual feedback.

Hydraulic drive [7]–[10] is another method that is often used to drive live line working robots due to its excellent insulation performance. However, many researchers chose Electrohydraulic mix-drive because it can easily achieve accurate control. ''ROBTET'' [7] is a robotic system consists of two hydraulic driven 6 DOF manipulators and is developed for outage-free maintenance tasks. This robot can work in a 69 kV substation. In recent years, Simas *et al.* [8] developed a hydraulic robot that is applied to power line insulator maintenance. It uses hydraulic cylinders to drive its joints and is designed to clean insulators of 13.8 kV distribution network poles. As in [9] and [10], a base-excited hydraulic manipulator system was used in live power line maintenance. This system has a 4-DOF slave Kodiak hydraulic manipulator that is installed on a 6-DOF Stewart platform to simulate the motion of a crane bucket in a real field. This robot system is a training system and is used to help linemen using robotics system effectively.

In a substation, the voltage is usually higher than 110 kV and can even reach 1000 kV in an ultrahigh voltage (UHV) substation. This leads to insulation and EMI problems [11], [12] and will make live working difficult.

The associate editor coordinating the review of this manuscript and approving it for publication was Xiao-Sheng Si.

A hydraulic mechanical arm can be relatively resistant to a higher voltage, but it is more likely to cause leakage and pollute the environment. Pneumatic equipment is more difficult to control than the former two types. However, for some tasks, such as insulator string carrying or cleaning, the insulation ability is more important than the precise motion. Another advantage of a pneumatic drive is that it is pollution free. Thus, the pneumatic drive robots could be a better choice for high voltage substation.

Many efficient and practical pneumatic actuators have been developed and put into application [13]–[16], such as pneumatic artificial muscles (PAMs) [13], [14], cylinder (rodless pneumatic actuator [15]), rotatory vane [16], air motor and so on. They all have different advantages. PAMs features low weight, has a high rate of power to weight, and can be used without reduction [13]. Rodless pneumatic actuators can achieve high dynamics of motion [15], and rotatory vanes [16] can output angle parameters directly without other structures compared with a cylinder

However, these pneumatic actuators need position sensors to constitute a closed loop control system. These electronic components are susceptible to EMI, and they could be damaged when used in an UHV substation. This paper proposes a pneumatic manipulator that is designed with no sensor feedback. The manipulator is driven by air motors and has no electrical connection with the controller and the manipulator. This design provides absolute electrical isolation between the operator and the manipulator and enables the manipulator to satisfy higher voltage applications. However, this approach will make it difficult for the operator to control the manipulator, and how to improve the usability of this manipulator is the main work for this paper.

To achieve better usability, we choose model predictive control (MPC) method to control the manipulator, and cameras are used as auxiliary tools. The MPC algorithm attempts to optimize future plant behavior by computing a sequence of future manipulated variable adjustments at each control interval [17]. Researchers have already used this method in special micro machines to meet the needs of special environments [18].

In this paper, the dynamic model of the wrist joint is established, and the state space equation, in which the pressure loss is contained, is proposed. Furthermore, the angle prediction model is established and used as a feedback signal to form the closed-loop control of the sensorless pneumatic joint.

This paper is structured as follows. In Section 2, the air motor driven manipulator that is designed for the live working environment is introduced. The dynamic model of the joint is presented in Section 3. In Section 4, the control algorithm of the system is given, including the control diagram and control platform. Finally, conclusions are drawn in Section 5.

II. DESCRIPTION OF THE MANUPULATOR

The designed pneumatic driving manipulator is shown in Fig. 1. The structural characteristics of the manipulator are as follows:

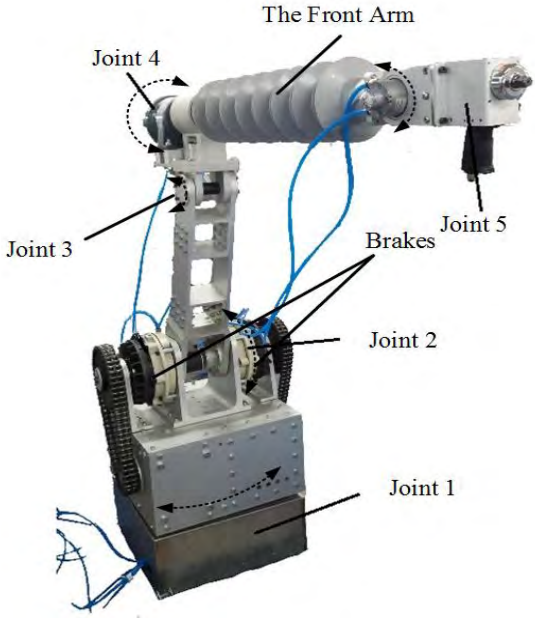

FIGURE 1. Five-degree-of-freedom manipulator experimental platform.

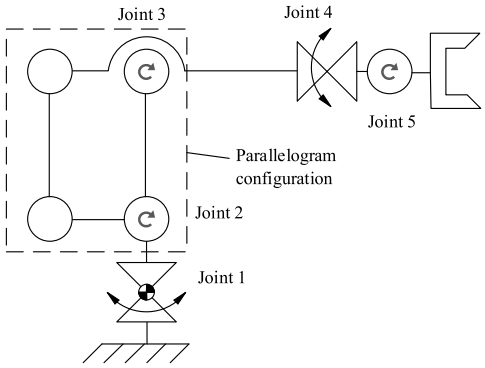

FIGURE 2. Diagram of the manipulator.

1) The manipulator has five joints, which are driven by pneumatic motors and can be locked by air brakes. Each of the five brakes is mounted on the side of a joint instead of the air motor to prevent the joint from malfunctioning and improve the response speed of a stop.
2) The front arm is made of glass fiber, and its outer surface is covered with a silicon umbrella type insulator to increase the creepage distance and improve the insulator ability.
3) There are no angle feedback units installed on the manipulator.
4) There are global cameras installed on the manipulator, and these cameras are self-powered.

The manipulator can reach a 1500-mm height and 1100- mm distance, and its maximum payload is 20 kg. As shown in Fig. 2, a parallelogram structure is used to increase the load while eliminating some of the coupling force.

This manipulator does not provide fully autonomous control, and the control schematic of pneumatic control is

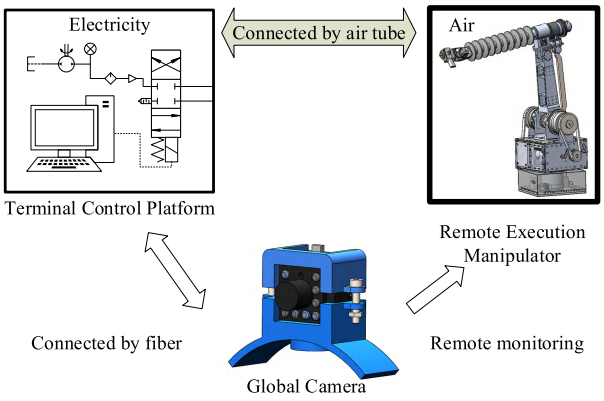

FIGURE 3. Platform control schematic.

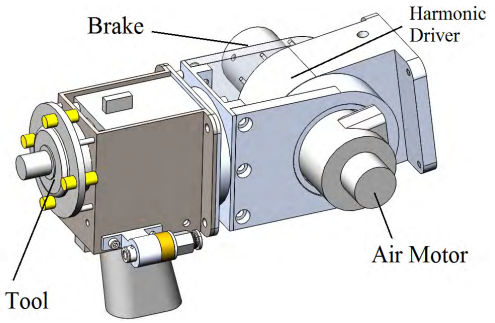

FIGURE 4. Model of the manipulator wrist.

illustrated in Fig. 3. The manipulator is connected with the remote control platform only by air pipeline and is controlled by the terminal control platform. This design ensures that the terminal control platform is insulated from the manipulator and improves the operator's safety during live working operations.

The terminal control platform includes a PC, solenoid valves, control handles and other control components.

This manipulator is designed to execute equipment maintenance tasks such as holding a brush to clean the suspension insulator string, and this type of task does not require a higher operation precision but will have a high risk of electric shock. Because there are no angle measuring instruments installed on it, the general motion control method cannot be used. When using this manipulator, lineman must operate the joints one after another with the aid of the overall-view camera.

In the actual operation process, because there are no angle measuring devices installed on the manipulator, it is difficult for the workers to operate. To reduce the operating complexity and improve the usability, we tried to establish a dynamic model of the pneumatic decelerating motors that can be used to predict the actual rotating angle of the joint at one step.

The wrist joint is the last joint and plays a key role for the manipulator to reach a desired position. In this study, we mainly aim at the control method for the wrist joint to ensure the accuracy of the end effector. Additionally, the control method can be applied to the other joints.

The wrist joint model is shown in Fig. 4. The transmission relationship diagram of the joint is shown in Fig. 5.

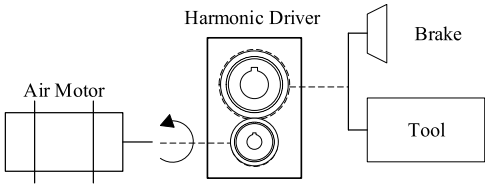

FIGURE 5. Establishment of the dynamic model of the wrist joint.

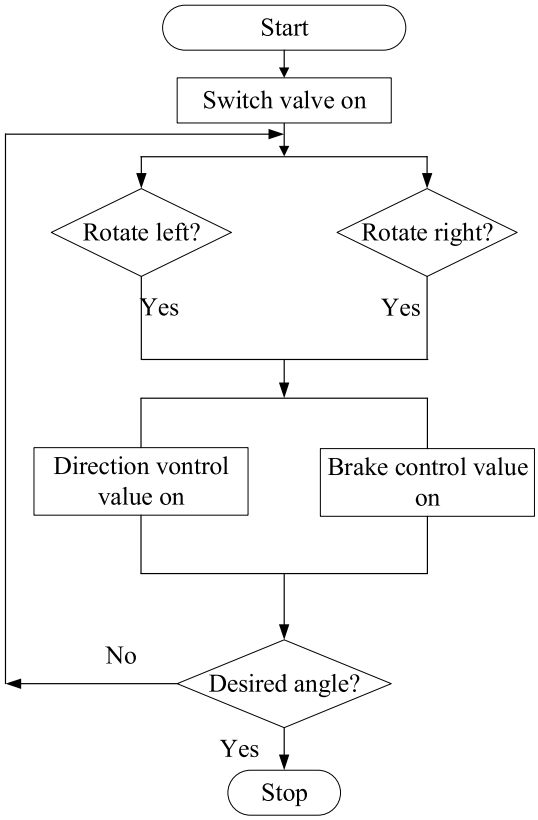

FIGURE 6. Control flowchart of joint.

A harmonic reducer is used for the wrist joint. The air brake is externally placed to prevent the end tool from falling and damaging the device when the air source is shut off.

III. ESTABLISHMENT OF THE DYNAMIC MODEL OF THE WRIST JOINT

In [20], an air motor model is established, which is mainly used to describe the rotation characteristics of the motor under constant input pressure, but the pressure loss of the control circuit is not considered. In our design, the air motor is far from the air pump, and the pressure loss cannot be neglected.

A. THE ESTABLISHMENT OF THE AIR PRESSURE LOSS MODEL

For the wrist joint, the control flowchart is presented in Fig. 6 and its pneumatic circuit diagram is shown in Fig. 7.

As shown in Fig. 6, the switch value will be turn on firstly to provide driving air for the brake and motor.

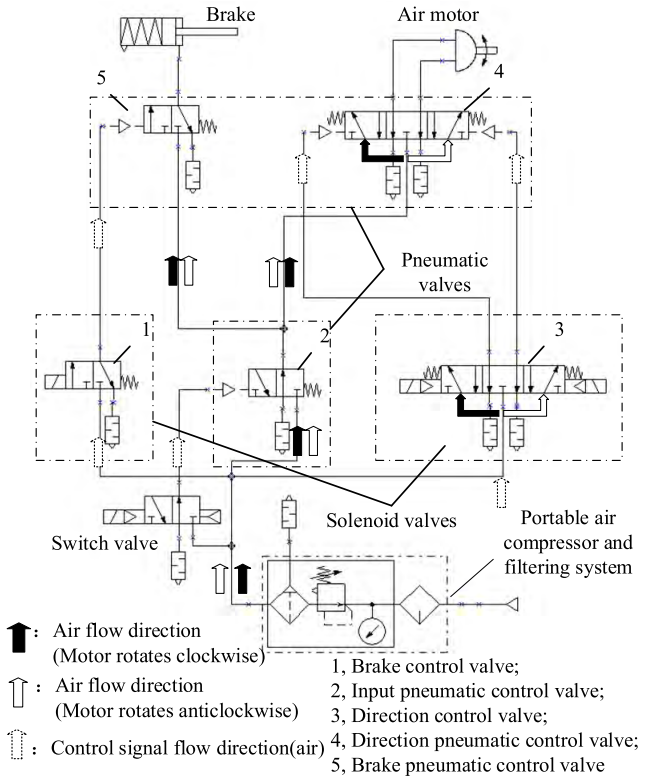

FIGURE 7. Pneumatic circuit diagram: 1-Brake control valve 2-Input pneumatic control valve 3-Direction control valve 4-Direction pneumatic control valve 5-Brake pneumatic control valve.

Then a control single will be given to the brake control value and direction control value, and the motor will turn clockwise or anticlockwise accordingly.

In Fig. 7, there are three solenoid valves and three pneumatic valves. Valve 2 is used to control the air flow into the brake and the air motor. Valves 1 and 5 play a role in controlling the brake. Valves 3 and 4 are combined to control the air motor. The control steps of the air motor are as follows:

–Firstly, the switch valve is turned on, the air motor and brake prepare to work.

– Secondly, the switch on signal is given. The solenoid valve 1 and switch valve are activated simultaneously.

–The body of the valve 4 moves to the left position, and the air motor rotate clockwise, and vice versa.

This pneumatic control system consists of solenoid valves and pneumatic valves. This structure can lengthen the distance between the remote control platform and the manipulator, which will improve the insulation property of the remote control platform.

According to the Darcy–Weisbach equation [22], the unit resistance loss R under different pressure and temperature can be described by

$$R = 23378\frac{\lambda V^2 T_m \rho_0}{d^5 P_m} \tag{1}$$

where λ is the flow coefficient, V is the volume flow rate under the standard state, T_{m} is the average temperature of the air, ρ_0 is the density of the air under the standard condition, d is the diameter of the air tube, and P_m is the average pressure of the pipeline, which can be defined by

$$P_m = (P_i + P_o)/2$$

where P_i is the output pressure of the air compressor, and P_o is the outlet pressure of the air motor.

In equation (1), T_{m} can be defined by

$$T_m = (T_B + T_o)/2$$

where T_B is the outlet temperature of the air motor and can be calculated from (2), and T_o is the temperature of the air tube end. T_B varies with the air pressure.

According to the isentropic process, T_B can be described as

$$T_B = T_s(\frac{P_B}{P_s})^{\frac{k-1}{k}} \tag{2}$$

where k is the ratio of the specific heat, and P_s is the source chamber pressure of the air motor. T_s is the initial temperature of the air source.

The flow coefficient λ is related to the Reynolds number Re. In this paper, Re = 2497, which is greater than 2100 and lower than 4000. Thus the flow is turbulent [23], and λ can be described as

$$\lambda = \frac{0.316}{\mathrm{Re}^{0.25}} \tag{3}$$

Then, the pipeline pressure loss can be written as

$$\begin{cases} \Delta P_i = L_i R = P_i - P_s \\ P_e = P_o \end{cases} \tag{4}$$

where L_i is the length of the input air pipe between the solenoid valve and the pneumatic motor, and P_e is the exhausted chamber pressure of the air motor.

Invoking (1) $\sim$ (4), the air pressure loss model can be written as

$$\begin{cases} P_s = P_i - 46756\frac{\lambda L_i V^2 T_m \rho_0}{d^5(P_i + P_o)} \\ P_e = P_o \end{cases} \tag{5}$$

B. THE ESTABLISHMENT OF THE JOINT MODEL

The simplified structure of the air motor is shown in Fig. 8. When establishing the model of the air motor, the moment of inertia for the air motor and harmonic reducer, the kinematic viscosity, sliding friction should be considered.

The model of the reducer can be defined as follows

$$\begin{cases} M_{\mathrm{o}} = M_i/i \\ \omega_o = i\omega_i \end{cases} \tag{6}$$

where i is the reduction ratio, M_o is the output torque, M_i is the input torque, ω_i is the input angular velocity, and ω_o is the output angular velocity.

As shown in Fig. 8, the compressed air can enter from port A or B and create a pressure difference between the

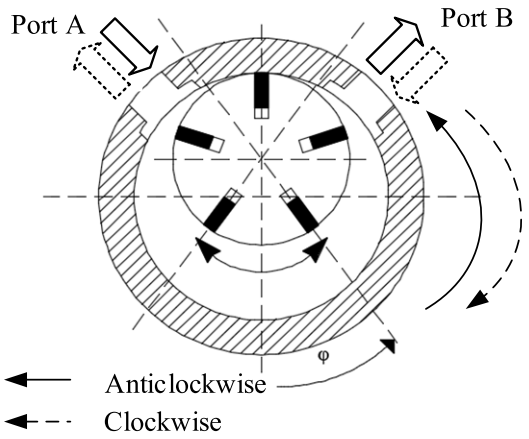

FIGURE 8. Air motor structure diagram.

two chambers. The air pressure pushes the blades to achieve positive and inverse rotation.

The following assumptions are adopted in this paper

1) There is no heat exchange between the motor chamber and the environment.
2) The outlet pressure of the gas source is constant, and the temperature of the gas source is 25°.
3) The thermal process of gas in the motor chamber is quasi-static.
4) The internal and external leakage of the motor can be ignored.
5) The working balance point of the air motor is at $\varphi = 0$.

According to the state space equation of the air motor [20], when considering the gas pressure loss and reduction ratio, the new state space equation of the air motor driving system can be described as follows:

$$\begin{cases} \dot{x}_1(t) = x_2(t) \\ \dot{x}_2(t) = \dfrac{L}{2Ji}(x_3 - x_4) \times (e^2 \cos 2\dfrac{x_1}{i} + 2eBcos\dfrac{x_1}{i} \\ \qquad +B^2 - r^2) - \dfrac{C_s}{J}S(x_2) - \dfrac{C_f}{J}x_2 \\ \dot{x}_3(t) = K_c \dfrac{A_A u_1(t) f(x_3(t), P_s, P_e)}{V_A(x_1(t))} \\ \qquad -\dfrac{k}{V_A(x_1(t))}\tilde{V}_A(x_1(t))x_2(t)x_3(t) \\ \dot{x}_4(t) = K_c \dfrac{A_B u_2(t) f(x_4(t), P_s, P_e)}{V_B(x_1(t))} \\ \qquad -\dfrac{k}{V_B(x_1(t))}\tilde{V}_B(x_1(t))x_2(t)x_4(t) \end{cases} \tag{7}$$

where $x_1(t)$, $x_2(t)$, $x_3(t)$ and $x_4(t)$ are the rotation angle of the output shaft, the velocity of the motor, and the pressure of the inlet chamber and outlet chamber, respectively. Additionally, u_1, u_2 and A_A, A_B are the control variables and the input parameters of the control valve. V_A, V_B are the control volumes of the driving and exhaust chamber, and their derivatives are $\tilde{V}_A$, $\tilde{V}_B$.

Considering the structure parameters of the reducer and air motor, when the motor rotates clockwise, V_A, V_B $\tilde{V}_A$ and $\tilde{V}_B$ can be calculated as

$$\begin{aligned} V_A(x_1(t)) &= \{162[\pi + (\frac{x_1}{i} - j\frac{\pi}{2})] + 0.0178 \sin\ 2(\frac{x_1}{i} - j\frac{\pi}{2}) \\ &\quad + 0.6497 \sin(\frac{x_1}{i} - j\frac{\pi}{2}) + 0.8072\} \times 10^{-5}; \\ V_B(x_1(t)) &= \{162[\pi - (\frac{x_1}{i} - j\frac{\pi}{2})] - 0.0178 \sin\ 2(\frac{x_1}{i} - j\frac{\pi}{2}) \\ &\quad - 0.6497 \sin(\frac{x_1}{i} - j\frac{\pi}{2}) - 0.8072\} \times 10^{-5}; \\ \tilde{V}_A(x_1(t)) &= \{162 + 0.0356 \cos 2(\frac{x_1}{i} - j\frac{\pi}{2}) \\ &\quad + 0.6497 \sin(\frac{x_1}{i} - j\frac{\pi}{2})\} \times 10^{-5}; \\ \tilde{V}_B(x_1(t)) &= -\tilde{V}_A(x_1(t)); \end{aligned}$$

When the motor rotates anticlockwise, V_A, V_B, $\tilde{V}_A$ and $\tilde{V}_B$ can be calculated as

$$\begin{aligned} V_A(x_1(t)) &= \{162[\pi - (\frac{x_1}{i} - (j+1)\frac{\pi}{2})] - 0.0178 \sin\ 2(\frac{x_1}{i} \\ &\quad -(j+1)\frac{\pi}{2}) - 0.6497 \sin(\frac{x_1}{i} - (j+1)\frac{\pi}{2}) \\ &\quad - 0.8072\} \times 10^{-5}; \\ V_B(x_1(t)) &= \{162[\pi + (\frac{x_1}{i} - (j+1)\frac{\pi}{2})] + 0.0178 \sin\ 2(\frac{x_1}{i} \\ &\quad -(j+1)\frac{\pi}{2}) + 0.6497 \sin(\frac{x_1}{i} - (j+1)\frac{\pi}{2}) \\ &\quad + 0.8072\} \times 10^{-5}; \\ \tilde{V}_A(x_1(t)) &= \{162 - 0.0356 \cos 2(\frac{x_1}{i} - (j+1)\frac{\pi}{2}) \\ &\quad -0.6497 \sin(\frac{x_1}{i} - (j+1)\frac{\pi}{2})\} \times 10^{-5}; \\ \tilde{V}_B(x_1(t)) &= -\tilde{V}_A(x_1(t)); \end{aligned}$$

According to the standard orifice theory [19], $\tilde{f}(P_r)$ can be calculated as

$$\tilde{f}(P_r) = \begin{cases} 1, & \dfrac{P_{atm}}{P_u} < P_r \leq 0.258 \\ 3.864[P_r^{2/k} - P_r^{(k+1)/k}], & 2058 < p_r < l_r \end{cases}$$

where P_s and P_e can be obtained from equation (5). In addition, $P_r = P_d / P_u$ is the ratio of the downstream pressure P_d and upstream pressure P_u at the orifice. P_{atm} is the atmospheric pressure, and P_{atm}=P_0.

The output equation can be described as

$$y = \begin{bmatrix} 1 & & & \\ & 0 & & \\ & & 0 & \\ & & & 0 \end{bmatrix} \begin{bmatrix} x_1 \\ x_2 \\ x_3 \\ x_4 \end{bmatrix}$$

When this predictive model is applied, the initial conditions need to be determined first (initial pressure and initial angle). Based on these conditions, the Runge-Kutta method is used to solve the mathematical model with the aid of the computer. The x_1, x_2, x_3, x_4 are calculated in each step, then the output y can be obtained.

The air motor type of the wrist is 1UP-NRV-3A, and the number of vanes is 4, the maximum power torque is 0.31Nm, and the maximum power speed is 6000rpm. The reducer type is LHS-17-120-C-I, and its reduction ratio is 1:120.

TABLE 1. The system parameters.

Symbol	Parameters	Value
i	Reduction ratio	120
C_s	Stiction coefficient	0.5 N
C_f	Friction coefficient	0.09 Ns
T_s	Temperature of the air source	293 K
R	Gas constant	287 J/(kg·K)
k	Ratio of specific heat	1.4
C_0	Flow constant	0.0404
C_d	Discharge coefficient	0.8
P_{atm}	Atmospheric pressure	0.101 MPa
λ	Flow coefficient	0.0447
J	Rotor's moment of inertia	0.0289 kgm^2
$K_c = kRT_sC_dC_0 = 3804.95$ J/kg		

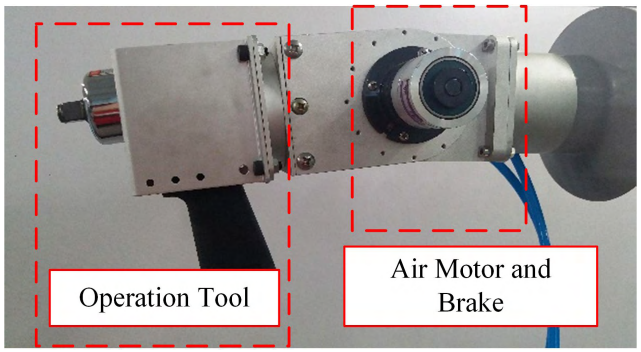

FIGURE 9. Pneumatic wrist joint.

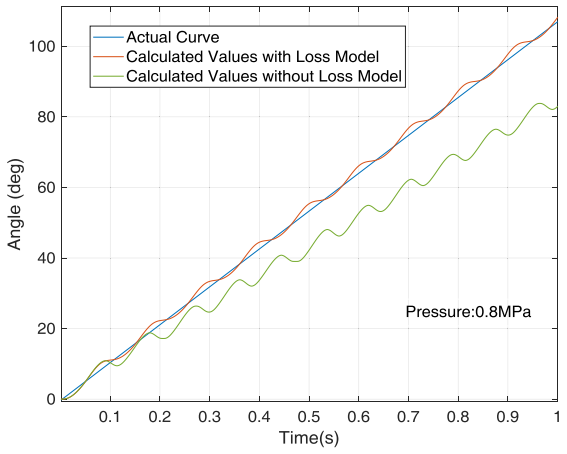

FIGURE 10. Computation of the rotation angles and experimental data at 0.8 MPa.

The system parameters are listed in Table 1.

To verify the validity of the dynamic model, the rotation experiment is executed. The wrist joint is shown in Fig. 9. The input pressure of the air is changed to different values in this experiment.

The working pressure of the air motor is from 0.5 MPa to 0.8 MPa. Thus, the experimental pressure is set to 0.8 MPa, 0.7 MPa, 0.6 MPa and 0.5 MPa, respectively.

The experimental data and the simulation data are shown in Fig. 10 to Fig. 13. In Fig. 10 to Fig. 13, if the pressure loss is not considered in the model, the maximum error of model is 6.1°, 22.3°, 27.2° and about 40°, respectively. The average error is 3.2°, 13.4°, 14.3° and 22.2°, respectively. While taking the pressure loss into account, the maximum

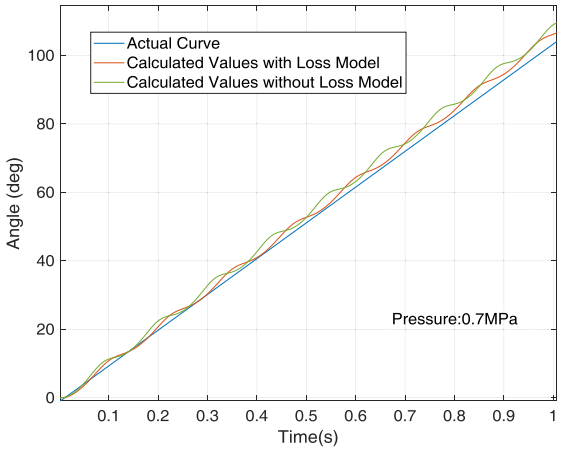

FIGURE 11. Computation of the rotation angles and experimental data at 0.7 MPa.

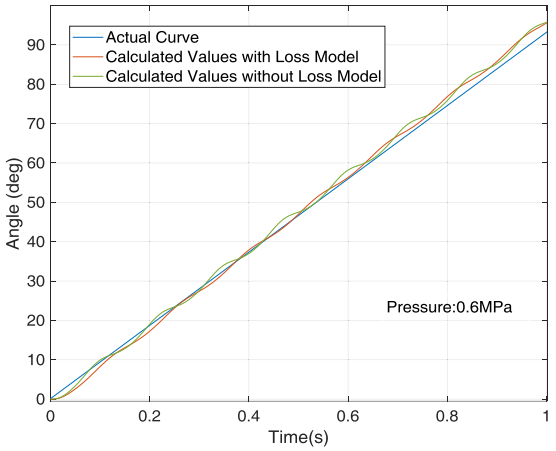

FIGURE 12. Computation of the rotation angles and experimental data at 0.6 MPa.

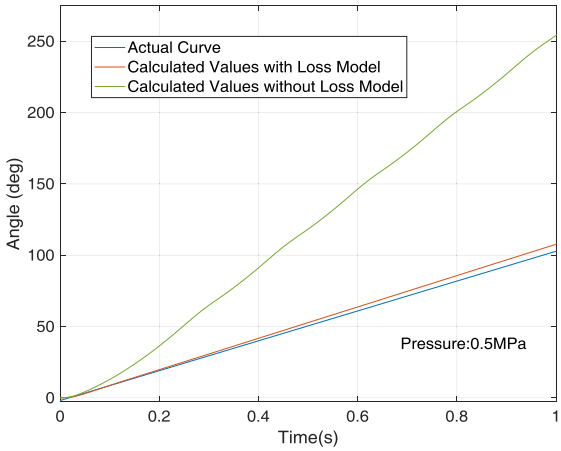

FIGURE 13. Computation of the rotation angles and experimental data at 0.5 MPa.

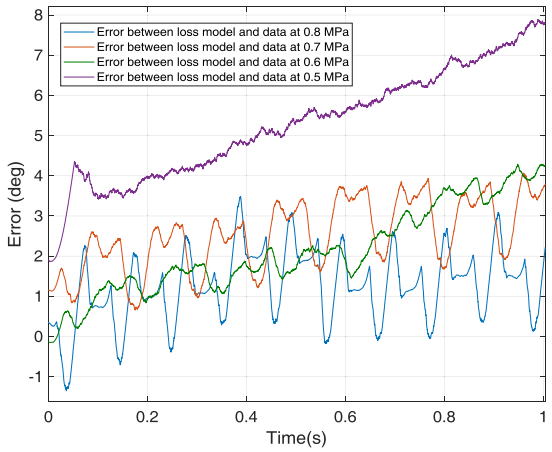

FIGURE 14. Error for the model with the loss model under different pressures.

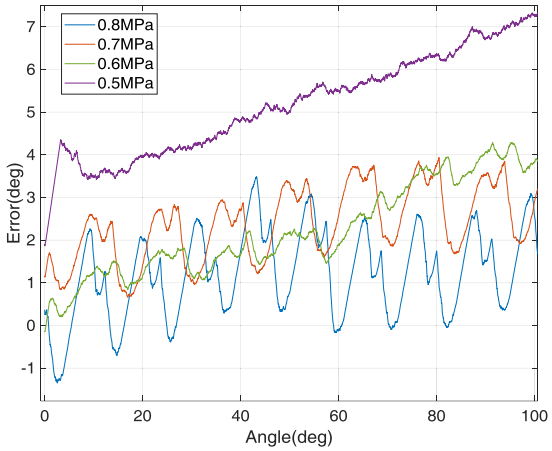

FIGURE 15. Error for the model with the loss model under different pressures at different angles.

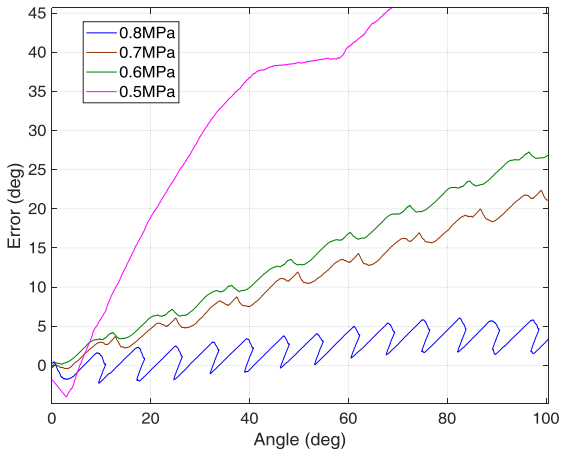

FIGURE 16. Error for the model without the loss model under different pressures at different angles.

error of model is 3.3°, 4.1°, 4.3° and 7.9°, respectively. The average error is 1.2°, 2.0°, 2.2° and 5.4°, respectively.

The deviation of experiment data is shown in Fig. 14 to Fig. 16.

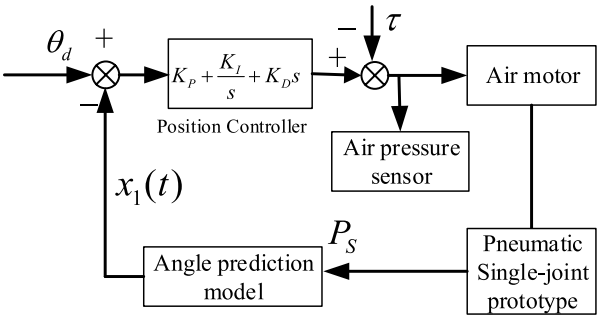

FIGURE 17. Feedback control scheme based on the angle prediction model.

The results of the experiment show the following:

1) For the model with pressure loss, the computation results are closer to the actual value. The accuracy of the model with pressure loss is higher than the model without pressure loss.
2) The error for the model with pressure loss increases as the pressure increases.
3) When the air pressure is higher than 0.7 MPa or lower than 0.6 MPa, the simulation results of the model without pressure loss have an apparent deviation from the actual value.
4) The deviation increases as the simulation time increases. Thus, the computation time must be under a limited value to ensure the operation's accuracy.
5) In a one second simulation, the max deviation increases as the pressure decreases.

IV. FEEDBACK CONTROL BASED ON THE ANGLE PREDICTION MODEL

In this section, the state space equations ($x_1(t)$, $x_2(t)$, $x_3(t)$ and $x_4(t)$) are used to establish the feedback control model.

The feedback control scheme based on the angle prediction model is shown in Fig. 17. In Fig. 17, Cτ is the external disturbance, and K_P, K_I, K_D are PID parameters, $x_1(t)$ is the predictive angle value of the model, and θ_d is the expected value.

The input pressure P_s is measured by the pressure sensor installed on the proportional valve.

By solving the angle prediction model, the predicted value of the actual angle $x_1(t)$ is obtained, and this value is used to realize the closed-loop control of the pneumatic joint.

Before obtaining the estimated angle value, the pressure should be transformed to the displacement of the valve body. The opening of the proportional valve is linear with the output pressure. They can be described by

$$u(t) = k_u P_v$$

where $u(t)$ is the valve body displacement, k_u is the proportional coefficient and is determined by experiment, $k_u = 0.1959$, P_v is the pressure measured by the pressure sensor.

This equation is used to convert the collected pressure value into the valve body displacement, and then the displacement is converted into the estimated angle value $x_1(t)$.

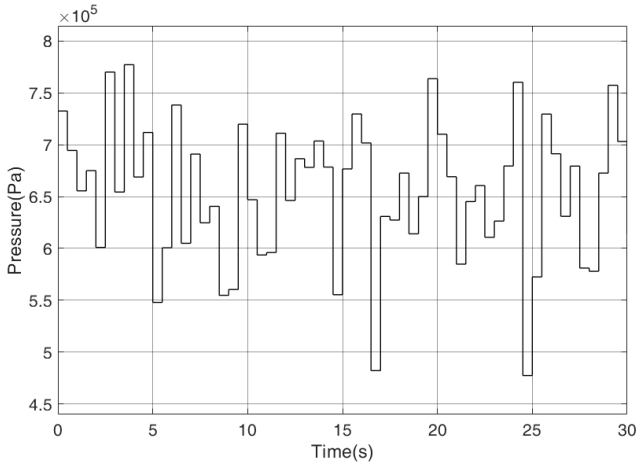

FIGURE 18. The random input pressure generated by the software.

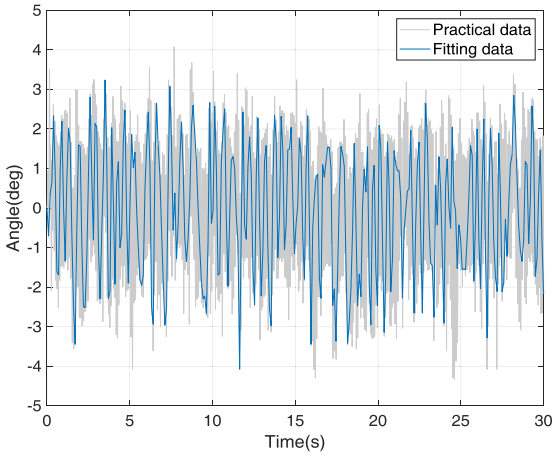

FIGURE 19. Control error under random pressures.

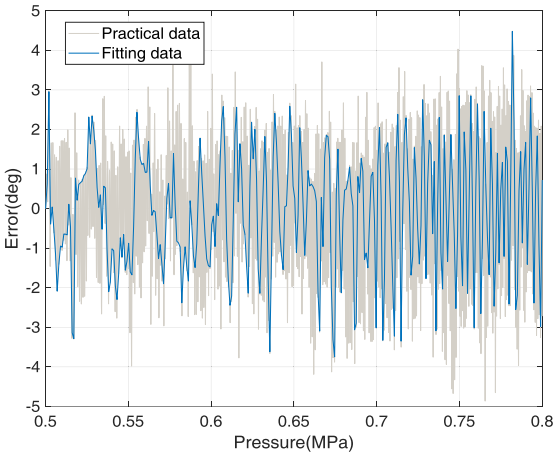

FIGURE 20. Control error under increasing pressures.

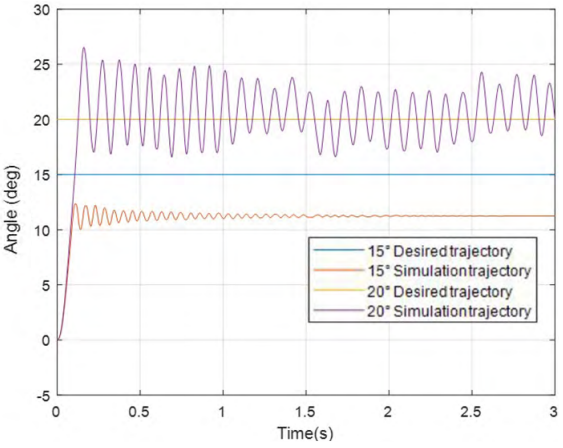

FIGURE 21. Minimum angle of rotation.

Before experiment, the sensibility of the control method is tested via simulation. As shown in the Fig. 18, the pressure value, which is randomly generated by the software, is input into the simulation system. To ensure the pressure value at the range of about 0.5MPa to 0.8MPa, the mean value of this pressure is set to 0.6MPa, while the variance is 5×10^9. The response time of the proportional valve is 0.1s. So the duration of each value is set to 0.5s to make the system reach the steady-state.

The sensitivity of the control for random variations in valve pressure is illustrated in Fig. 19. The initial and desire pose angle is set to 0°. The experimental time is 30s.

The pose error measured in the manual operation experiment is 8.35° in average. Fig. 19 shows that the maximum pose error is 4.33°, this means that this control method is insensitive to the pressure and can reduce the pose error.

The control error under different pressure is also shown in Fig. 20. The control error increase with the pressure increasing. A higher pressure can make the system response more quickly but less accurate. This means that the low pressure needs a lager opening of valve, and the error can be controlled to a low level. So in this condition, the error could be limited to the range of $-3° \sim 3°$ under 0.5MPa.

The system takes the angle predictor output as its feedback. Base on this approach, a control model was built to simulate the joint at a pressure of 0.5 MPa.

In fact, when the joint is controlled to a small angle, a small opening is needed. So insufficient air pressure will make the air motor unable to lift the load. The simulation results show that there is a minimum identification angle. As shown in Fig. 21, when the rotation angle is less than 20°, the system will lose its dynamic adjustment capability. Therefore, the joint should be controlled above 20°, for each time of rotation. When the rotation angle is less than 20°, the joint can be manually controlled.

The experimental platform is illustrated in Fig. 22. There is a proportional valve, solenoid valves and a supply power.

The slewing area of the wrist joint is from $-90°$, to 90°. Considering the symmetries of slewing area, the rotation angle of the wrist joint is set to 20°, 21°, 22°, and so on, up to 90°, at the pressure of 0.5MPa, and the error between the simulation results and the desired angle is calculated and illustrated in Fig. 23.

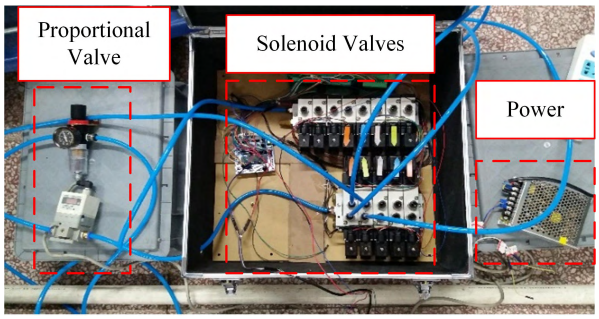

FIGURE 22. Single joint control principle experimental verification platform.

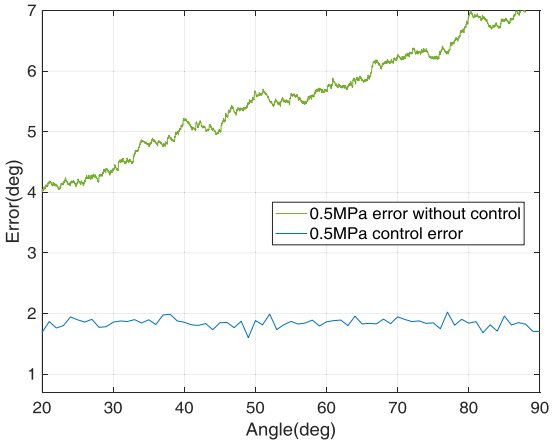

FIGURE 23. Feedback and no feedback control error.

Fig. 23 shows that with the increase of the rotation angle, the error of the open-loop control method and close-loop control method will increase. In this experiment, the error of the open-loop control varies from 4.04°, to 7.18°, and the error of the close-loop control varies from 1.60°, to 2.02°. Compared with the open-loop control error, the average error of the closed-loop control is reduced to 1.84°. So this predictor feedback control method can be a better method to control this type of manipulator.

In summary, the application of this predictive feedback control method can be used between 20°, and 90°, to achieve better accuracy. When the rotation angle is less than 20°, it can be adjusted by manual operation.

V. CONCLUSION

To improve the usability of the wrist joint of an air motor drove manipulator, the wrist joint dynamic model include air pressure loss is established. This dynamic model is used to predict the rotation angle of the wrist joint. Furthermore, the dynamic model is also used in a model predictive control method to reach a higher control accuracy. The experimental results show the following:

1) The dynamic model with air pressure loss can be a good method to predict the actual rotation angle for this type application.
2) The model predictive control method can accomplish a higher accuracy.
3) When using this model predictive control method, the rotation angle should be set above 20°.
4) When the rotation angle is under 20°, it can be accomplished manually.
5) For this type of application, the air pressure loss must be considered in the model of the joint.

It is difficult for this angle predictive algorithm to reach a high positioning accuracy, but it can be an effective method to ease the use of this type of manipulator which can realize perfect insulation capability under high voltage environment. In respect of the safety and reliability, this provides a novel idea when designing live work automation equipment. In our future work, this control algorithm will be applied to the other joints to ease the use of the manipulator. Furthermore, the dynamic model will be simplified to reduce the calculation time.

REFERENCES

[1] R. S. Gonçalves and J. C. M. Carvalho, "Review and latest trends in mobile robots used on power transmission lines," *Int. J. Adv. Robotic Syst.*, vol. 10, no. 12, p. 408, 2013.
[2] M. Nakashima, H. Yakabe, Y. Maruyama, K. Yano, K. Morita, and H. Nakagaki, "Application of semi-automatic robot technology on hot-line maintenance work," in *Proc. IEEE Int. Conf. Robot. Automat.*, Nagoya, Japan, vol. 1, May 1995, pp. 843–850.
[3] E. J. Lima, M. H. S. Bomfim, and M. A. D. Mourao, "POLIBOT—POwer lines inspection RoBOT," (in English), *Ind. Robot, Int. J.*, vol. 45, no. 1, pp. 98–109, 2018.
[4] J.-Y. Park, J.-K. Lee, B.-H. Cho, and K.-Y. Oh, "An inspection robot for live-line suspension insulator strings in 345-kV power lines," *IEEE Trans. Power Del.*, vol. 27, no. 2, pp. 632–639, Apr. 2012.
[5] W. Jiang *et al.*, "Structure singular value theory based robust motion control of live maintenance robot with reconfigurable terminal function for high voltage transmission line," (in English), *Int. J. Adv. Robotic Syst.*, vol. 15, no. 2, p. 17, Apr. 2018.
[6] K. Tsukahara *et al.*, "An experimental robot system for power distribution line maintenance robots—System architecture and bolt insertion experiment," in *Proc. IEEE/RSJ Int. Conf. Intell. Robots Syst.*, Sep. 2008, pp. 1730–1736.
[7] R. Aracil, M. Ferre, M. Hernando, E. Pinto, and J. M. Sebastian, "Telerobotic system for live-power line maintenance: ROBTET," *Control Eng. Pract.*, vol. 10, no. 11, pp. 1271–1281, 2002.
[8] H. Simas *et al.*, "Kinematic conception of a hydraulic robot applied to power line insulators maintenance," in *Proc. 20th Cobem-Int. Congr. Mechanocal Eng.*, vol. 4, 2009, pp. 739–748.
[9] V. Banthia, Y. Maddahi, S. Balakrishnan, and N. Sepehri, "Haptic-enabled teleoperation of base-excited hydraulic manipulators applied to live-line maintenance," in *Proc. IEEE/RSJ Int. Conf. Intell. Robots Syst.*, Sep. 2014, pp. 1222–1229.
[10] Y. Maddahi, K. Zareinia, T. Olson, W. Mueller, and N. Sepehri, "Live-line maintenance training using robotics technology," in *Proc. World Haptics Conf.*, Apr. 2013, pp. 587–592.
[11] C. A. Silveira, G. M. Fonseca, C. A. Costa, R. R. B. Aquino, and L. H. A. de Medeiros, "Analyzing low frequency couplings in substations under steady-state conditions: Part I," in *Proc. IEEE/PES Transmision Distrib. Conf. Expo., Latin Amer.*, Nov. 2004, pp. 737–742.
[12] C. A. Silveira, G. M. Fonseca, R. R. B. Aquino, and L. H. A. de Medeiros, "Analyzing low frequency couplings in substations under steady-state conditions: Part II," in *Proc. IEEE/PES Transmision Distrib. Conf. Expo., Latin Amer.*, Nov. 2004, pp. 731–736.
[13] A. Hošovský, J. Pitel, K. Židek, M. Tóthová, J. Sárosi, and L. Cveticanin, "Dynamic characterization and simulation of two-link soft robot arm with pneumatic muscles," (in English), *Mechanism Mach. Theory*, vol. 103, pp. 98–116, Sep. 2016.
[14] K. K. Ahn and H. T. C. Nguyen, "Intelligent switching control of a pneumatic muscle robot arm using learning vector quantization neural network," *Mechatronics*, vol. 17, no. 4, pp. 255–262, 2015.

[15] P. A. Laski, J. E. Takosoglu, and S. Blasiak, "Design of a 3-DOF tripod electro-pneumatic parallel manipulator," *Robot. Auton. Syst.*, vol. 72, pp. 59–70, Oct. 2015.
[16] Festo.com. (2017). *BionicCobot*. Accessed: Dec. 16, 2017. [Online]. Available: https://www.festo.com/group/en/cms/12746.htm
[17] S. J. Qin and T. A. Badgwell, "A survey of industrial model predictive control technology," *Control Eng. Pract.*, vol. 11, no. 7, pp. 733–764, 2003.
[18] W. Wang, L. Yu, J. Yang, and Y. Yan, "Full closed-loop position control of the surgical cable-driven micromanipulator based on joint angle estimator," *Robot*, vol. 40, no. 2, pp. 231–239, 2018.
[19] G. M. Bone, M. Xue, and J. Flett, "Position control of hybrid pneumatic–electric actuators using discrete-valued model-predictive control," *Mechatronics*, vol. 25, pp. 1–10, Feb. 2015.
[20] X. Luo, J. Wang, L. Shpanin, N. Jia, G. Liu, and A. S. I. Zinober, "Development of a mathematical model for vane-type air motors with arbitrary *N* vanes," in *Proc. World Congr. Eng.*, London, U.K., vol. 1, Jul. 2008, pp. 1–6.
[21] F. Takemura, R. S. Pandian, Y. Hayakawa, and S. Kawamura, "Modeling and sliding mode control of a vane type pneumatic motor," *Jpn. Soc. Mech. Eng., Trans. C*, vol. 66, no. 652, pp. 127–134, 2000.
[22] E. G. Harris, "Friction in air pipes," in *Compressed Air-Theory and Computations*, 1st ed. New York, NY, USA: McGraw-Hill, 1910, pp. 33–35. [Online]. Available: http://www.ebooksread.com/authors-eng/elmo-golightly-harris/compressed-air-theory-and-computations-hci.shtml
[23] F. M. White, "Viscous flow in ducts," in *Fluid Mechnics*, 7th ed. New York, NY, USA: McGraw-Hill, 2011, pp. 347–352.
[24] W. Durfee, "Basic principles of fluid power," in *Fluid Power System Dynamics*. Mnineapolis, MN, USA: Univ. of Minnesota, 2015, pp. 20–25. [Online]. Available: https://sites.google.com/site/fluidpoweropencourseware/library
[25] J. Wang, J. Pu, P. R. Moore, and Z. Zhang, "Modelling study and servo-control of air motor systems," *Int. J. Control*, vol. 71, no. 3, pp. 459–476, 1998.
[26] J. Gaspar-Badillo, J. Ramos-Arreguin, G. Macias-Bobadilla, D. Talavera-Velazquez, E. Rivas-Araiza, and H. Víctor-Alexis, "Four DOF pneumatic robot design and hardware interface," in *Proc. 13th Int. Eng. Congr. (CONIIN)*, Santiago de Queretaro, Mexico, May 2017, pp. 1–7.

YANHENG ZHANG received the B.S. degree in mechanical engineering from Shandong University, Jinan, Shandong, China, in 2000, the M.S. degree in mechanical engineering from the Qingdao University of Science and Technology, Qingdao, Shandong, in 2003, and the Ph.D. degree in mechanical engineering from Beihang University, Beijing, China, in 2007. He is currently an Associate Professor with the Automation School, Beijing University of Posts and Telecommunications, Beijing, China. His research interests include spherical robot, modular manipulator, mechanism design, and pipe robot.

XIE CHEN received the B.S. degree in mechanical engineering and automation from Shanghai University (SHU), Shanghai, China, in 2016, and the M.S. degree in mechanical engineering from the Beijing University of Posts and Telecommunications, Beijing, China. His research interests include manipulator, pneumatic actuator, and mechanism design and control.

HUIZHI WANG received the B.S. degree from the South China University of Technology (SCUT), Guangdong, China, in 2015, and the M.S. degree in mechanical engineering from the Beijing University of Posts and Telecommunications, Beijing, China. His research interests include manipulator, pneumatic actuator, and mechanism design and control.

LUFENG ZHANG received the B.S. degree in mechanical design manufacturing and automation from the East China University of Science and Technology (ECUST), Shanghai, China, in 2015, and the M.S. degree in mechanical engineering from the Beijing University of Posts and Telecommunications, Beijing, China. His research interests include mobile robot, jumping robot, and mechanism design and control.